AFRL-VS-HA-TR-2004-1029

IMPROVED SURFACE WAVE DISPERSION MODELS AND AMPLITUDE MEASUREMENTS

J. L. Stevens
D. A. Adams
M. G. Eneva
G. R. Baker

Science Applications International Corporation
10260 Campus Point Drive
San Diego, CA 92121-1578

24 October 2003

Scientific Report No. 2

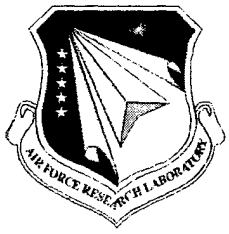

AIR FORCE RESEARCH LABORATORY
Space Vehicles Directorate
29 Randolph Rd
AIR FORCE MATERIEL COMMAND
Hanscom AFB, MA 01731-3010

This technical report has been reviewed and is approved for publication.

/SIGNED/	/SIGNED/
ROBERT RAISTRICK	ROBERT BELAND
Contract Manager	Branch Chief

This document has been reviewed by the ESC Public Affairs Office and has been approved for release to the National Technical Information Service (NTIS).

Qualified requestors may obtain additional copies from the Defense Technical Information Center (DTIC). All others should apply to the NTIS.

If your address has changed, if you with to be removed from the mailing list, or if the addressee is no longer employed by your organization, please notify AFRL/VSIM, 29 Randolph Rd., Hanscom AFB, MA 01731-3010. This will assist us in maintaining a current mailing list.

Do not return copies of this report unless contractual obligations or notices on a specific document require that it be returned.

REPORT DOCUMENTATION PAGE

Form Approved
OMB No. 0704-0188

1. REPORT DATE *(DD-MM-YYYY)*	2. REPORT TYPE	3. DATES COVERED *(From - To)*
24-10-2003	SCIENTIFIC REPORT # 2	1 Oct 02 - 30 Sep 03

4. TITLE AND SUBTITLE
Improved Surface Wave Dispersion Models and Amplitude Measurements

5a. CONTRACT NUMBER
DTRA01-01-C-0082

5b. GRANT NUMBER

5c. PROGRAM ELEMENT NUMBER

6. AUTHOR(S)
J.L. Stevens, D.A. Adams, M.G. Eneva, and G.E. Baker

5d. PROJECT NUMBER
DTRA

5e. TASK NUMBER
OT

5f. WORK UNIT NUMBER
A1

7. PERFORMING ORGANIZATION NAME(S) AND ADDRESS(ES)
Science Applications International Corporation
10260 Campus Point Drive
San Diego, CA 92121-1578

8. PERFORMING ORGANIZATION REPORT NUMBER
SAIC-03/2051

9. SPONSORING / MONITORING AGENCY NAME(S) AND ADDRESS(ES)
Air Force Research Laboratory
29 Randolph Road
Hanscom AFB MA 01731-3010

10. SPONSOR/MONITOR'S ACRONYM(S)
AFRL/VSBYE

11. SPONSOR/MONITOR'S REPORT NUMBER(S)
AFRL-VS-HA-TR-2004-1029

12. DISTRIBUTION / AVAILABILITY STATEMENT
Approved for Public Release; Distribution Unlimited

13. SUPPLEMENTARY NOTES

14. ABSTRACT
The report describes the status and results to reduce the magnitude threshold for which surface waves can be identified and measured reliably, and to improve the accuracy of surface wave measurements, using phase-matched filtering, development of global regionalized earth and dispersion models, and other techniques. We have focused on improvements to global earth models and dispersion maps, and improved techniques for measuring surface wave amplitudes. Completed work on implementation and testing of azimuth estimation techniques at three component stations based on polarization analysis. Global regionalized earth and dispersion models are being developed by inversion of the very large data set of phase and group velocity dispersion measurements. The complete data set now contains over one million dispersion data points. The dispersion measurements are inverted for earth structure; the earth structure is then used to generate dispersion predictions. Improvement in the inversion procedure has been the introduction of the capability to vary damping and smoothing parameters for each model.

15. SUBJECT TERMS
Seismic velocity Seismic attenuation Seismic propagation

16. SECURITY CLASSIFICATION OF:			17. LIMITATION OF ABSTRACT	18. NUMBER OF PAGES	19a. NAME OF RESPONSIBLE PERSON
a. REPORT	b. ABSTRACT	c. THIS PAGE			Robert Raistrick
UNCLAS	UNCLAS	UNCLAS	SAR		19b. TELEPHONE NUMBER *(include area code)* 781 377-3726

CONTENTS

Section **Page**

ABSTRACT

The report describes the status and results at the end of the second year of a project to reduce the magnitude threshold for which surface waves can be identified and measured reliably, and to improve the accuracy of surface wave measurement, using phase-matched filtering, development of global regionalized earth and dispersion models, and other techniques. In year two, we have focused on two topics: improvements to global earth models and dispersion maps, and improved techniques for measuring surface wave amplitudes. We also completed work on implementation and testing of azimuth estimation techniques at three component stations based on polarization analysis. Global regionalized earth and dispersion models are being developed by inversion of a very large data set of phase and group velocity dispersion measurements. The complete data set now contains over one million dispersion data points. The dispersion measurements are inverted for earth structure, and the earth structure is then used to generate dispersion predictions. A significant improvement in the inversion procedure over the past year has been the introduction of the capability to vary damping and smoothing parameters for each model. This allows us to improve the data fit for many models, while still retaining realistic earth models in all areas. In addition to improving earth and dispersion models, we have implemented and tested procedures for measuring surface wave amplitudes at short periods (5-15 seconds) and at regional distances. We find that the best procedure is to measure surface wave amplitudes at periods greater than 12 seconds at all distance ranges for three reasons: 1) earthquake spectra tend to decrease with frequency, degrading discrimination; 2) unlike time domain measurements, spectral measurements can be made accurately at lower frequencies at close distances; and 3) S/N remains higher at periods greater than 12 seconds even for very close distances.

LIST OF FIGURES

Page

LIST OF TABLES

Page

PREFACE

We would like to thank Mike Ritzwoller, Anatoli Levshin and Nikolai Shapiro of the University of Colorado, Bob Herrmann of St. Louis University, and other researchers who have allowed us to use their data in this project.

1. EXECUTIVE SUMMARY

Surface waves are of primary importance for nuclear monitoring because the M_s:m_b discriminant and its regional variants are among the most reliable means of determining whether an event is an earthquake or an explosion. The primary goal of this project is to reduce the magnitude threshold for which surface waves can be identified and measured reliably and to improve the accuracy of surface wave measurement using phase-matched filtering and global regionalized earth and dispersion models.

Global regionalized earth and dispersion models are being developed by inversion of a very large data set of phase and group velocity dispersion measurements. The complete data set now contains over one million dispersion data points. The dispersion measurements are inverted for earth structure, and the earth structure is then used to generate dispersion predictions. This is accomplished in the following way. The inversion is performed for approximately 600 distinct base structures, which were originally derived from the Crust 2.0 models over the AK135 mantle model. The Moho depth, bathymetry, and sediment depths vary on a one-degree grid. Moho depths are derived from Crust 2.0, sediment depths from the Laske and Masters sediment maps, and bathymetry from ETOPO5. Moho depth, bathymetry, and sediment properties are fixed in the inversion, while crust and upper mantle velocities are allowed to vary in the base models. Phase and group velocity dispersion curves are calculated for each of 64,800 models on the one-degree grid. The phase velocity dispersion curves are then used to calculate phase-matched filters to improve detection.

One of the difficulties of performing such a large, heterogeneous inversion is finding optimum values for smoothing and damping (regularizing) parameters. This is important because too much smoothing/damping will increase data misfit, and too little will produce unrealistic earth models. In this case, smoothing minimizes the gradient of each structure between specified discontinuities, while damping minimizes the difference between the model and the starting model. Discontinuities occur at the Moho and at the base of the surface sediments. In a few cases where there is sufficient high frequency information to resolve shallower structure, inversion is performed for deeper sediments, which introduces another discontinuity. A significant improvement in the inversion procedure over the past year has been the introduction of the capability to vary damping and smoothing parameters for each model. This allows us to improve the data fit for many models, while still retaining realistic earth models in all areas. We are performing 2D inversions (inversion of dispersion at discrete frequencies to form spatial dispersion maps) to identify regions where additional parameterization is needed in the 3D inversions. The additional parameterization takes the form of introduction of new base structures, merging of base structures, or adjustments to boundaries between base structures.

In addition to improving earth and dispersion models, we have implemented and tested procedures for measuring surface wave amplitudes at short periods (5-15 seconds) and at regional distances. We are identifying optimum procedures for measuring path corrected spectral magnitudes and then comparing the results with other procedures, such as Marshall-Basham amplitude corrections, which were designed to correct time domain amplitudes for frequency and structure dependence. Path corrected spectral magnitudes should be independent of distance and only weakly dependent on frequency for shallow events. At higher frequencies and longer distances the amplitude correction depends on having accurate Q models. We find that the best

procedure is to measure surface wave amplitudes at periods greater than 12 seconds at all distance ranges for three reasons: 1) earthquake spectra tend to decrease with frequency, degrading discrimination; 2) unlike time domain measurements, spectral measurements can be made accurately at lower frequencies at close distances; and 3) S/N remains higher at periods greater than 12 seconds even for very close distances.

We evaluate the performance of a new algorithm for determining Rayleigh wave propagation direction using the Rayleigh wave polarization. The algorithm uses the correlation of the horizontal and Hilbert transformed vertical seismograms to estimate backazimuth, where the horizontal component is rotated through the full range of possible backazimuths. The vertical and radial seismograms' correlation coefficient predicts the accuracy of the backazimuth estimate. The effect on backazimuth residuals of group velocity window, passband, and different measures of peak correlation, is evaluated using a large data set. We find that the algorithm provides accurate estimates of Rayleigh wave polarization and is a significant improvement over current automatic processing procedures. The algorithm can be combined with a dispersion test to improve detection capability.

2. GLOBAL EARTH MODELS AND SURFACE WAVE DISPERSION MAPS

To improve the detection and measurement of surface waves it is important to make good dispersion predictions. Dispersion is used in two ways: 1) to construct phase-matched filters to improve signal to noise ratio, and 2) to provide sufficient time resolution to test that the surface wave is correctly associated with a particular event. In our work, surface wave dispersion predictions are based on dispersion measurements for ray paths from all over the globe. We make these predictions via models of the earth. Alternate methods could be developed which would depend on interpolation schemes, such as kriging and which would not make use of earth models. An important advantage gained from using earth models is that we can include information from other studies leading to physically reasonable constraints on dispersion. For our earth models this information consists of the boundaries between geologic zones, bathymetry of oceans, thicknesses of sediments and ice, Moho depths, and prior estimates of seismic velocities derived from Crust 2.0 and AK 135 earth models. These constraints are especially important for filling in the gaps found in the path coverage of our data set and they enable prediction along paths unlike any of the paths in the data set. We perform non-linear least squares inversion of the dispersion data for two types of models. First are 3D earth models where the adjustable parameters are the shear wave velocities of layers. Second are 2D group velocity models determined by inverting dispersion measurements made in narrow frequency bands. The 2D models are used as a guide in the parameterization of the 3D earth model.

2.1 Description of 3D earth model

The 3D earth model is described briefly here and in greater detail in Stevens et al. (2002). It consists of 1°x1° blocks and is made up of layers of ice, water, sediments, crust and upper mantle. Currently this model depends on 8918 free parameters which are adjusted by least squares fitting to Rayleigh wave dispersion data. The free parameters are the S-wave velocities of layers of 572 different model types. Other constrained parameters in the model are P wave velocities, densities and Q. The model types are based on the Crust 2.0 2°x2° crustal types (Bassin et al., 2000 and Laske et al. 2001) and also on ocean ages (Stevens and Adams, 2000). The top few km of the model (consisting of water, ice and/or sediments) are fixed and match data from one degree bathymetry maps made by averaging Etopo5 five minute measurements of topography, and Laske and Masters (1997) 1 degree maps of sediments. There is an explicit discontinuity between the bottom of the sediments and the crust. There are three or more crustal layers. The Crust 2.0 models which were the starting point for these structures have three crustal layers, but we found it necessary to add more layers in regions of thick crust. There is another explicit discontinuity at the Crust/Mantle boundary. The Moho depth is derived from Crust 2.0 and varies on a 2° grid. The mantle starting model is derived from AK135 (Kennett, et al, 1995). With these constraints, the inversion is performed for the shear velocity of the crust and upper mantle to a depth of 300 km. Below 300 km the earth structure is fixed, and the inversion model is required to be continuous with the mantle structure at the base of the inversion. In broad ocean areas, we replace the Crust 2.0 model with models distinct for each ocean and subdivided by ocean age. We also separate into distinct models Crust 2.0 models that are geographically separated. So, for example, if Crust 2.0 has the same model type in North America and in Asia, we use the same starting model for each, but treat them as separate models in the inversion.

2.2 Surface wave dispersion data set

During the second year of our project we added three new sets of dispersion data and improved one already existing set bringing the total number of Rayleigh wave dispersion measurements with frequencies greater than or equal to .01 Hz to more than 1,000,000. One new set comes from Los Alamos National Laboratory (Yang et al, 2002) consisting of more than 37,000 dispersion measurements (2009 individual paths) from Central Asia ranging between 0.05 Hz and 0.23 Hz. For frequencies below 0.03 Hz these data are much slower than other data in the same region; consequently we have removed all the Los Alamos data below 0.04 Hz. Another set comes from Huang et al (2003) and consists of more than 285,000 data points (9730 paths) from China. These data include unrealistically fast paths crossing cells with water at frequencies higher than about 0.06 Hz. Consequently we have removed all the Huang data points with paths passing through cells with water above 0.04 Hz. We have added approximately 14,000 our own dispersion measurements for paths to IMS stations crossing Eurasia (Levshin et al, 2003). Pre-existing data coming from University of Colorado (Levshin et al, 2002) were improved by relocating events to the hypocenters in Engdahl et al (1998) where possible as described in Levshin et al. (2003). Other data already in the data set are described in Stevens et al (2001a,b and 2002). Figure 1 shows the frequency distribution of group velocity and phase measurements in our data set. In addition to the phase velocity measurements shown in the figure, the data set also includes a large number of long period phase velocities derived from the global phase velocity model of Ekstrom et al. (1996).

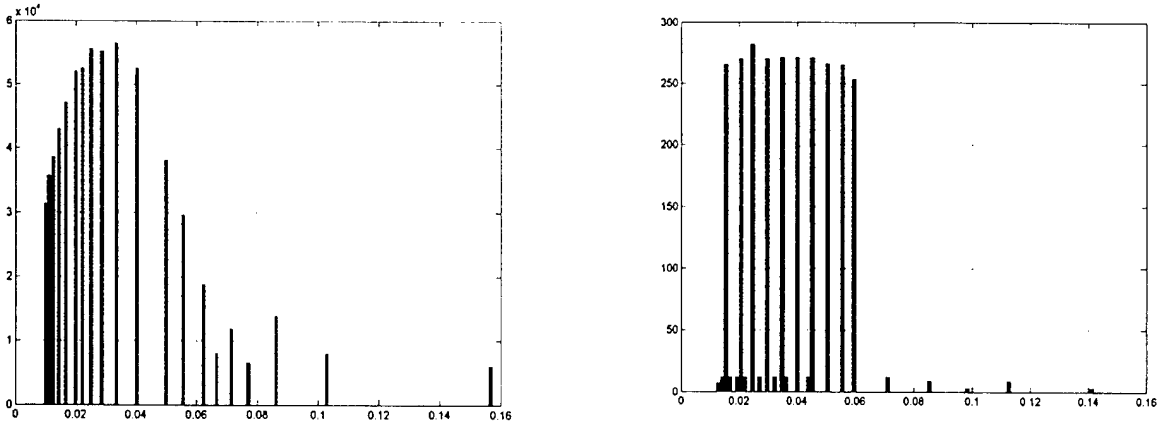

Figure 1. Bar graph of the number of group velocity measurements (left) and phase velocity measurements (right) in each frequency band for all data currently used in the tomographic inversions.

2.3 The inversion procedure for the 3D earth model

The relationship between dispersion and the shear wave velocities of the layers in the earth model is non-linear, so the shear wave velocities are estimated by non-linear least squares. At each step a system of tomographic equations is formed, augmented by additional equations of constraint and then solved by the LSQR algorithm. The equations solved are

$$\begin{pmatrix} A \\ sH \\ \lambda I \end{pmatrix} \vec{x} = \begin{pmatrix} \vec{l} \\ -sH\vec{x}_0 \\ -\lambda\vec{x}_0 \end{pmatrix} + \vec{\varepsilon},$$

where $\mathbf{x}$ is the vector of slowness adjustments to the shear wave slownesses of layers in each of the 572 model types. $\mathbf{l}$ is the vector of slowness differences between predicted and observed dispersion measurements. $\boldsymbol{\varepsilon}$ is the vector of residuals that remain after inversion (the inversion minimizes $|\boldsymbol{\varepsilon}|$). $\mathbf{x}_0$ is the vector of slownesses estimated in the last iteration. The elements of the matrix $\mathbf{A}$ consist of partial derivatives of dispersion predictions with respect to shear wave slownesses in each layer. $\mathbf{H}$ is a difference operator that applies to vertically neighboring layers and has the effect of constraining the vertical smoothness of velocity profile. $\mathbf{s}$ is the weighting of the smoothness constraint and can be a diagonal matrix (for variably weighted smoothing) or a scalar (constant smoothing). We have implemented variable smoothing so that a different smoothing parameter can be selected for each model type. Lateral smoothing, which is usually applied in tomography studies, is executed indirectly in our study through selection of the model types. $\mathbf{I}$ is the identity matrix and λ weights the damping which constrains the norm of the difference between final slownesses and constraining model slownesses (in our work a variant of the Crust 2.0 values). λ can be a scalar for constant damping, or a diagonal matrix for variable damping. As for smoothing, variable damping is implemented so that a different parameter can be selected for each model type.

2.4 Regularization and predictions

Choosing regularizing parameters is an essential part of finding a model which best predicts dispersion, since regularization acts both to control the influence of data noise on the estimation of model parameters and to constrain parts of the model that are poorly constrained by data. Too much regularization will make the model too smooth and too little regularization will allow noise to be projected into the model, making it unrealistic and rough. In this study the damping and smoothing constraints and their associated weighting parameters are used to regularize the solution. Techniques for optimization of regularization parameters are not yet mature, especially for large scale problems such as this. The methods most often described (e.g. Hansen, 1998) are the L-curve, generalized cross validation, and discrepancy principle. In the literature the first two methods are usually applied to smaller scale problems than ours and with only one regularizing parameter, whereas we have at least 2 and possibly many more. The last method mentioned requires a reliable independent estimate of data noise and works by selecting the regularization resulting in the residual based estimate of noise being the same as the independent estimate. We have experimented with several of these techniques for our inversion problem, but have not found any reliable enough to replace analyst review of the inversion results.

2.5 Techniques for evolving earth models

The selection of model types and regularizing parameters are interrelated. For example making a parameterization finer (i.e. adding new model types) without increasing data coverage increases the need for regularization. Our approach for finding a best predictive model has been to start with a small number of model types and increase this number gradually as new data become available or when we detect systematic data misfit. Once a new parameterization is determined, the regularizing parameters are adjusted.

To determine whether there are enough model types, we carry out 2D inversions of group velocity residuals in at least 12 narrow frequency bands to determine group velocity adjustment maps at 1-degree resolution. Each 2D inversion of group velocity residuals is regularized with a damping parameter which constrains the norm of the group velocity adjustment, and a smoothing

parameter which weights a first difference operator that constrains lateral smoothness of the estimated group velocity (i.e. $v+\delta v$). We vary these two parameters for each frequency band to find the smoothest looking map that still reduces data misfit reasonably. The resulting maps are examined to find areas of similar adjustment common to most frequency bands, which are then used to delineate new model types.

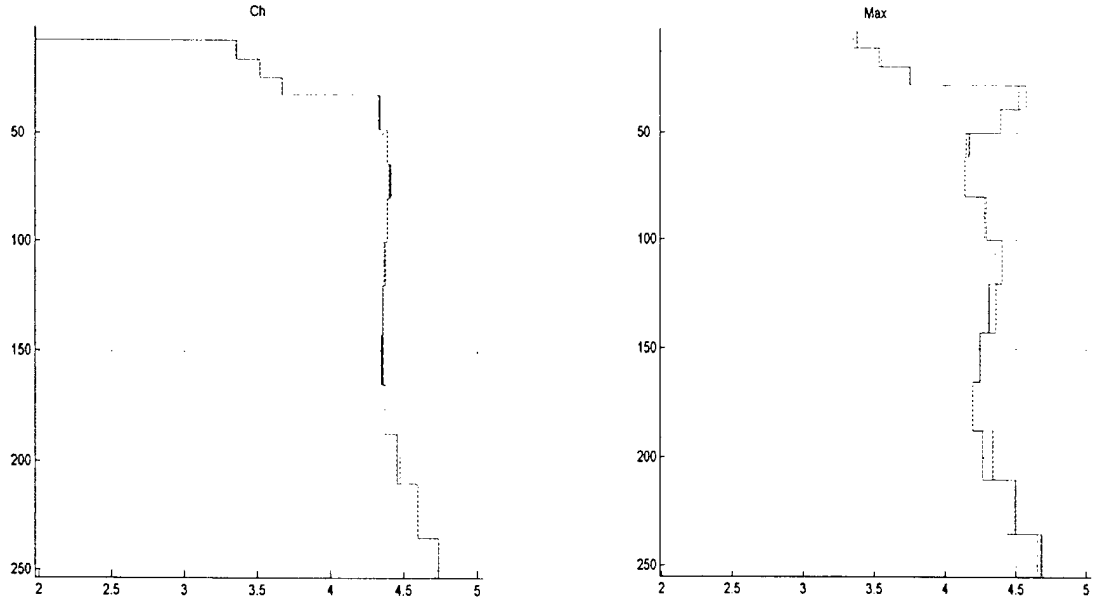

Figure 2. Shear velocity profiles for two model types: less sensitive to regularization on the left and more sensitive on the right. Ch is from the Yellow Sea and Max is from North East of Mexico. The different structures correspond to different combinations of the scalar regularization parameters s and λ.

After the model types are selected the damping and smoothing parameters (scalars, or diagonal matrices) $\boldsymbol{\lambda}$ and $\mathbf{s}$ are adjusted to find a reasonable looking model that still fits the data adequately. Currently we are experimenting with spatially variable regularization using diagonal matrices rather than scalars. We find that the sensitivity of slowness adjustments to scalar regularization parameter settings is not uniform and depends on model type. In other words when comparing adjustments for different combinations of scalar pairs (s, λ), there is much less variation for some model types than others (see for example Figure 2). The strategy we are now developing is to relax regularization for those types that are relatively insensitive to regularization, and to increase it for those model types that are sensitive to it.

A measure of sensitivity to regularization is the maximum of the absolute adjustments in S-wave slownesses (max_dev) for one or more regularizations. For example the map in Figure 3 shows how this deviation varies geographically when (s, λ)= (50,50). The map shows that oceanic model types are under regularized compared to the others. Several regularizations with $\mathbf{s}$ and $\boldsymbol{\lambda}$ diagonal matrices were formed where ($\mathbf{s}$(i), $\boldsymbol{\lambda}$(i)) = $\mathbf{a}$*K*max_dev(i), "i" indicates model type, $\mathbf{s}$(i) and $\boldsymbol{\lambda}$(i) are diagonal matrices with dimension equal to the number of adjustable layers in the i-th model, and K is a constant. K was varied to find its best value by comparing solutions. The vector $\mathbf{a}$ is (1,1) or (2,1). After a good value of K is found a small number of model types are still too sensitive, and for them the regularization needed to be increased further. Figure 4 shows maximum absolute deviations for the latest non-uniform regularization. Here the absolute deviations are much more similar among model types than in the uniform regularization case.

Figure 3. Map of maximum absolute slowness deviations (units of 10^{-3}) for each model type for a uniform regularization of (s, λ)= (50,50).

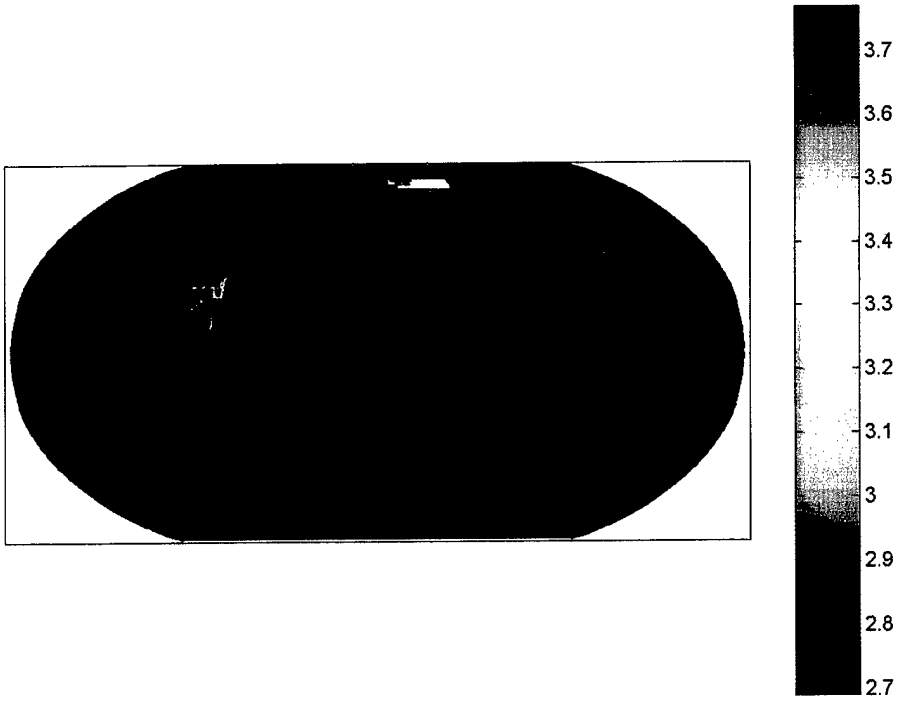

Figure 4. Map of maximum absolute slowness deviations (units of 10^{-3}) for each model type for most recent model type dependent (non-uniform) regularization .

2.6 Data statistics for best current 3D earth model

The means and standard deviations of normalized group velocity residuals, $1-v_o/v_p$, where v_o and v_p are observed and model predicted group velocities, were calculated for narrow frequency bands and are shown in Figure 5. Solid is for our best 1-degree model, and dashed is for the best 5-degree model (e.g. Stevens and Adams, 2000) based on Crust 5.1 (Mooney, et al., 1998). Figure 5 shows the value of the 1-degree model, especially for high frequencies.

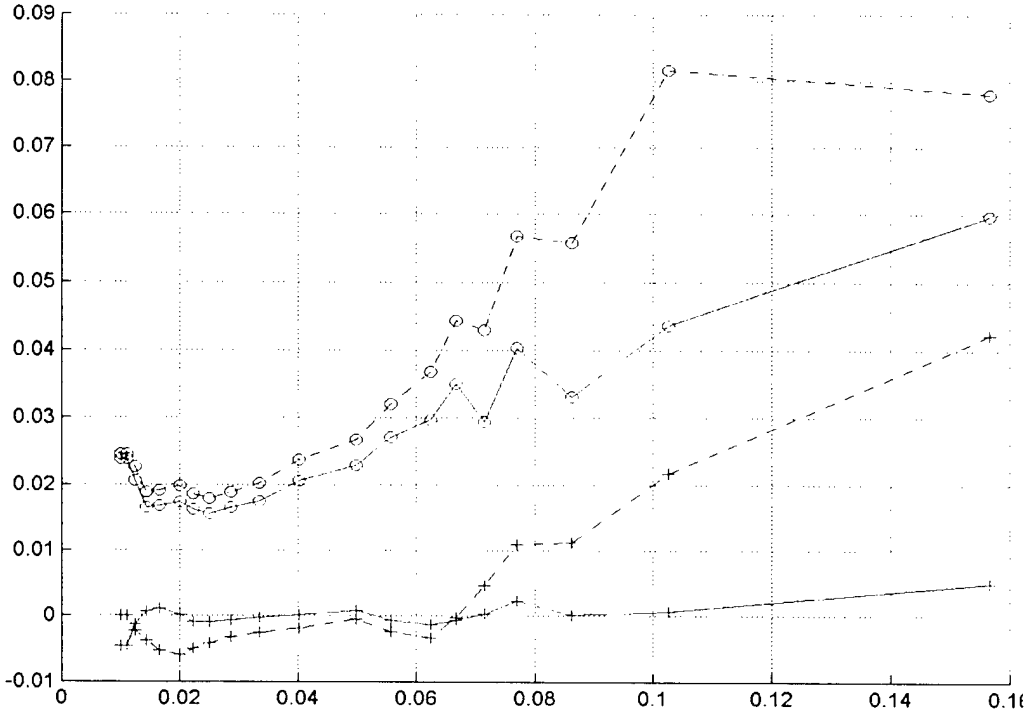

Figure 5. Standard deviations (o) and means (+) of normalized group velocity residuals are plotted against frequency for 1degree earth model (solid red) and 5-degree earth model (dashed blue).

3. OPTIMIZATION OF SURFACE WAVE AMPLITUDE MEASUREMENTS

Surface wave measurements traditionally are accomplished by measuring a time domain amplitude at a period near 20 seconds and then calculating a surface wave magnitude M_S. This procedure is problematic at regional distances because the surface wave is not well dispersed and a distinct 20-second arrival may not be present. It is possible to measure time domain amplitudes at higher frequencies with corrections (e.g. Marshall and Basham, 1972), however measurements may be inaccurate due to differences in dispersion caused by differences in earth structure. Stevens and McLaughlin (2001) suggested as an alternative replacing time domain measurements with a path corrected spectral magnitude. The path corrected spectral magnitude, $\log M_0$, is calculated by dividing the observed surface wave spectrum by the Green's function for an explosion of unit moment and taking the logarithm of this ratio, averaged over any desired frequency band. The objectives of the present study include determining the optimum frequency band for measurement and the best procedure for averaging the spectra over this band.

The advantages of using $\log M_0$ instead of the traditional surface wave magnitude M_S are that $\log M_0$ is insensitive to dispersion, independent of distance, works well at regional distances, and is inherently regionalizeable. Regionalized path corrected spectral magnitudes incorporate geographic variations in source excitation and attenuation. Furthermore, as discussed below, it can in principle be measured over different frequency bands to optimize the signal-to-noise ratio. M_S and $\log M_0$ share some limitations: spectra from earthquakes vary due to source mechanism and depth, and errors can occur if the measurement is made in a spectral dip or at high frequencies for a deep event (Figure 6). Azimuthal variations in amplitude caused by focal mechanism also affect the amplitudes of both $\log M_0$ and M_S.

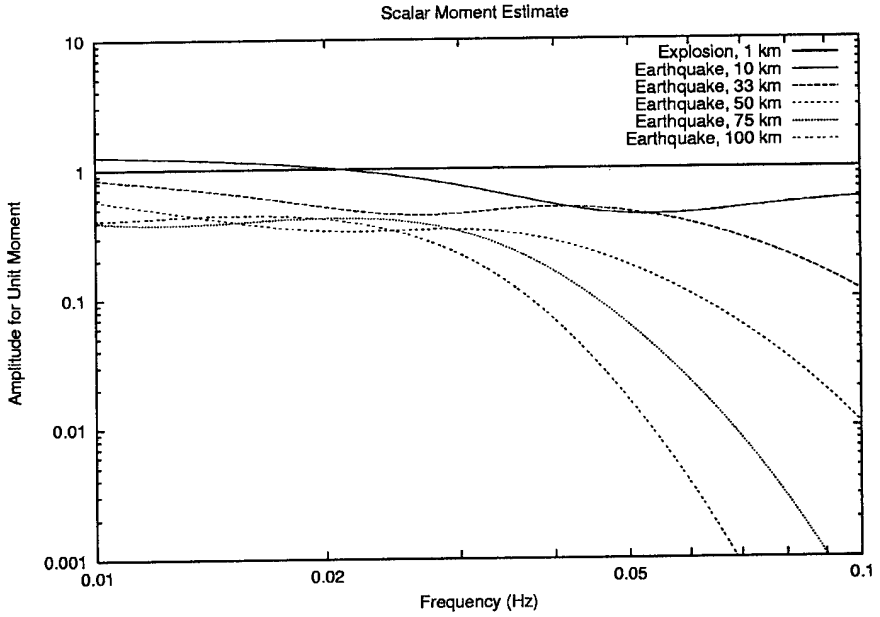

Figure 6. Path corrected spectral magnitude for an explosion and for earthquakes calculated for several depths. The path corrected explosion spectrum is flat over the entire frequency band (for perfect data and path correction, while the path corrected earthquake spectrum is flattened, but has some variation due to source mechanism and source depth.

The test cases discussed by Stevens and McLaughlin (2001) used a frequency band of 0.02-0.05 s (50-20 s) to estimate the spectral magnitudes. They estimated that on average, the time domain and spectral magnitudes are related as $\log M_0 = M_s + 11.75$. Most of the waveforms in that work were recorded at distances exceeding 8^0. Due to the relatively flat spectra over the 0.02-0.05 Hz band for most data, this choice worked quite well. The authors noted, however, that higher frequencies might be required for shorter paths. An important observation was that the $\log M_0$ residuals are independent of distance, despite the simple Q models used in the earth structures (Figure 7).

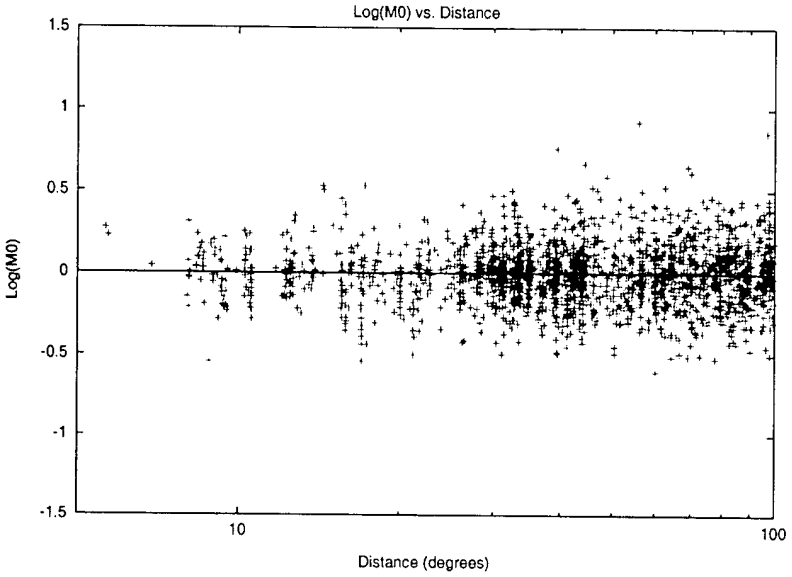

Figure 7. Path corrected spectral magnitude (Log M0) residuals plotted vs. distance (from Stevens and McLaughlin, 2001). Log M0 is nearly independent of distance.

In the present work we focus on the utility of higher frequencies in estimating spectral magnitudes of smaller events, recorded at smaller distances. The purpose is to optimize the spectral magnitude estimates, to test their distance and frequency independence, and to identify any measurement problems or pitfalls. For large amplitude signals we can expect the lower frequencies to be better in general, particularly at larger distances due to greater attenuation at higher frequencies. Our hypothesis at the initiation of this study was that using higher frequencies for measuring spectral magnitudes at shorter distances would optimize signal to noise ratio and therefore be better for measuring surface waves at regional distances, however as discussed below this is only true to a limited extent.

3.1 Surface wave measurements using events on and near the Lop Nor test site

To optimize the measurement procedures and examine the performance of the path corrected spectral magnitude at regional distances, we use 584 spectra from 76 earthquakes and 11 explosions in the Lop Nor area (Figure 8). Additional spectra are available from these events, but only the above spectra were deemed to be of good quality. This means that they passed the dispersion test described by Stevens and McLaughlin (2001) and were checked for certain anomalies such as incorrect instrument calibrations. Approximately 11% of the spectra used for the $\log M_0$ estimates originate from records at source-station distances of 5^0 or less, and another 11% at distances of 30^0 or greater. Thus the bulk of the data comes from intermediate distances. Figure 9 shows examples of explosion and earthquake path corrected spectra from Lop Nor at

various distances. The tendency of the explosion spectra to be relatively flat over more extended frequency bands compared with earthquake spectra is evident. This is expected because 1) the spectra are corrected by an explosion Green's function that flattens earthquake spectra imperfectly, and 2) the earthquake spectra have frequency variations caused by source mechanism and depth.

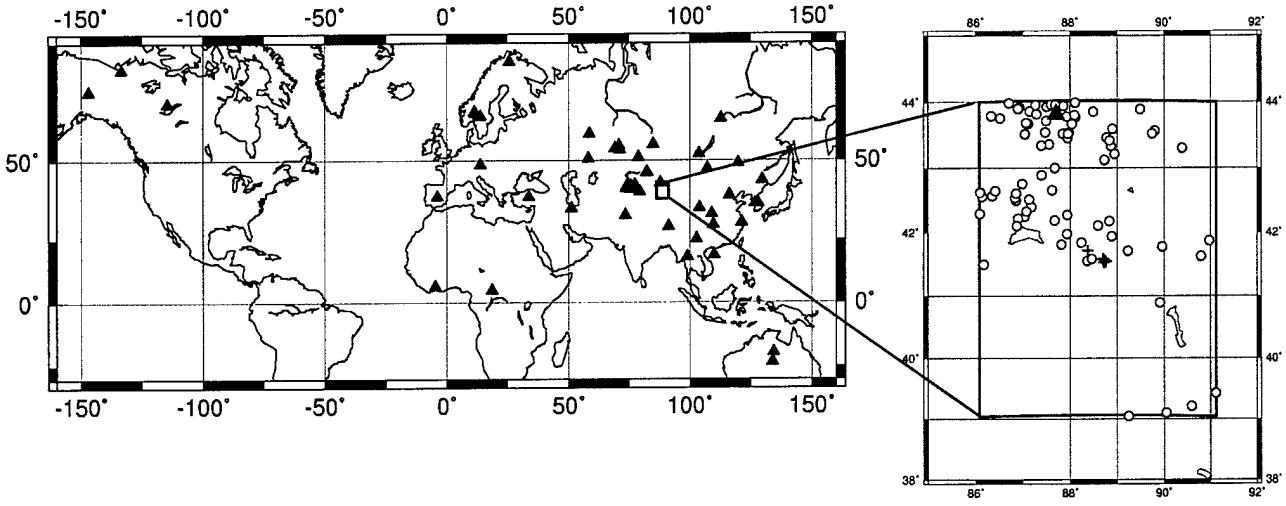

Figure 8. Maps showing the Lop Nor area (rectangle), stations (triangles), and earthquake (circles) and explosion (crosses) epicenters.

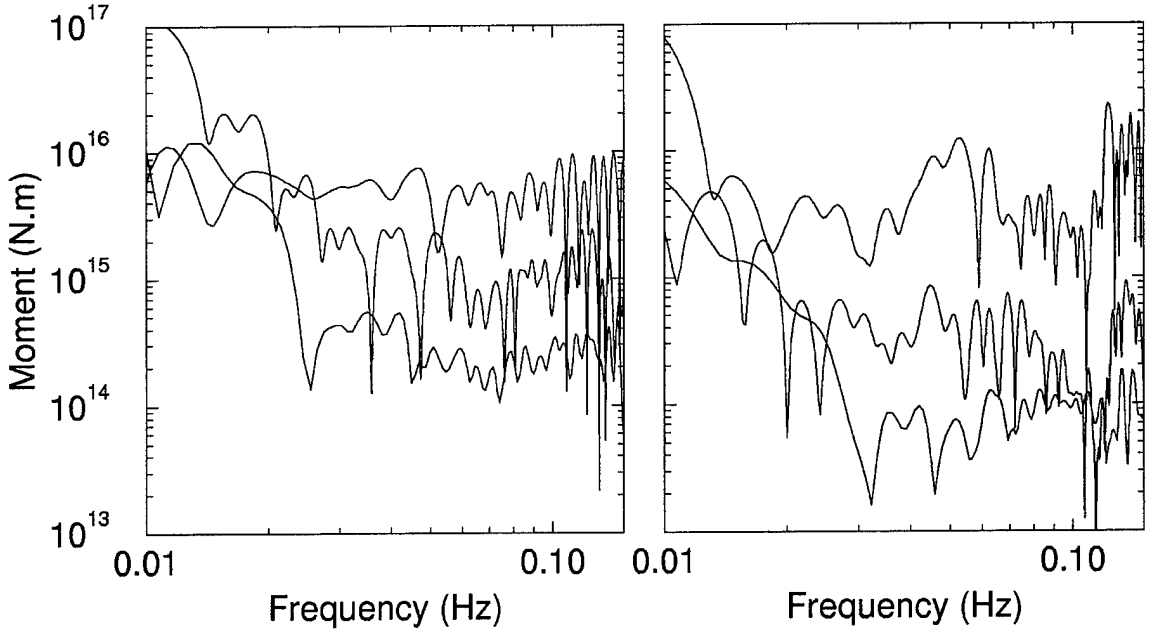

Figure 9. Examples of path corrected spectra used in this work: (a) Lop Nor explosions recorded at distances of 2°, 7° and 67° (left); (b) Lop Nor earthquakes recorded at distances of 0.4°, 22° and 65° (right). See examples of station $\log M_0$ estimates in Table 1. S/N is good at all but the highest frequencies. Low frequency noise dominates over the surface wave signal below about 0.02 Hz.

We calculated individual spectral magnitudes (i.e., several station magnitudes per event) over all possible frequency bands between 0.02 Hz (50 s) and 0.15 Hz (~7s), with bandwidths of 0.03 Hz, 0.04 Hz, etc., up to 0.13 Hz for the 0.02-0.15 Hz band. This procedure provided 153 bands to examine from each spectrum. In the search for the most robust spectral magnitude estimate, four different methods were used as follows.

1. Calculating a "simple" mean of the logarithms of all path corrected amplitude measurements made in a given frequency band. This is comparable to Stevens and McLaughlin's (2001) estimates in the 0.02-0.05 Hz band.

2. Iteratively calculating a "robust" mean, by rejecting outliers outside two standard deviations from the mean calculated at each step. The procedure ends when all measurements remain within two standard deviations or when half of the amplitude measurements in a frequency band are rejected, whichever occurs first. Thus the spectral magnitude estimates are much less affected adversely by the tendency of some spectra to sharply vary in amplitude over some frequencies, with most outliers marking anomalously low amplitudes (see Figure 9 above). Figure 10 compares the individual (station) $\log M_0$ estimates from (1) and (2). Standard deviations from the robust-mean method are predictably lower than those in the simple-mean method, as the insets in Figure 10 show.

3. Calculating $\log M_0$ at the center frequency of a least-squares straight line fit to the spectrum over a given frequency band.

4. Same as (3), but the straight line is "robust", minimizing the absolute deviations of the logarithms of the amplitudes from the line.

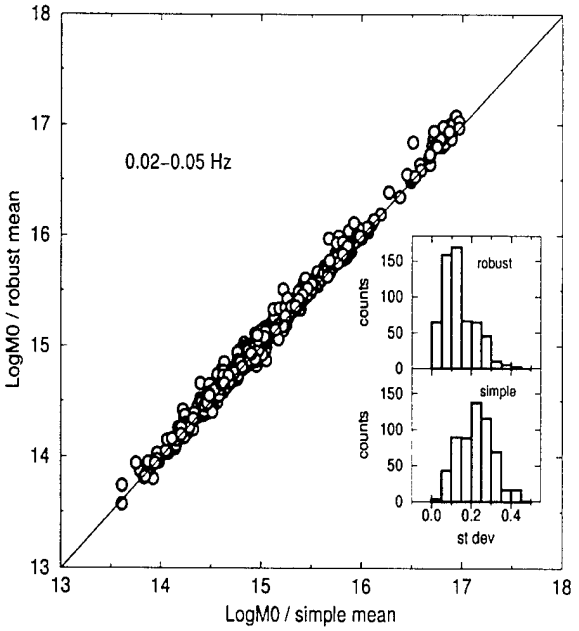

Figure 10. Comparison of station spectral magnitudes calculated with two different methods. Insets show standard deviations as indicated. See text for details.

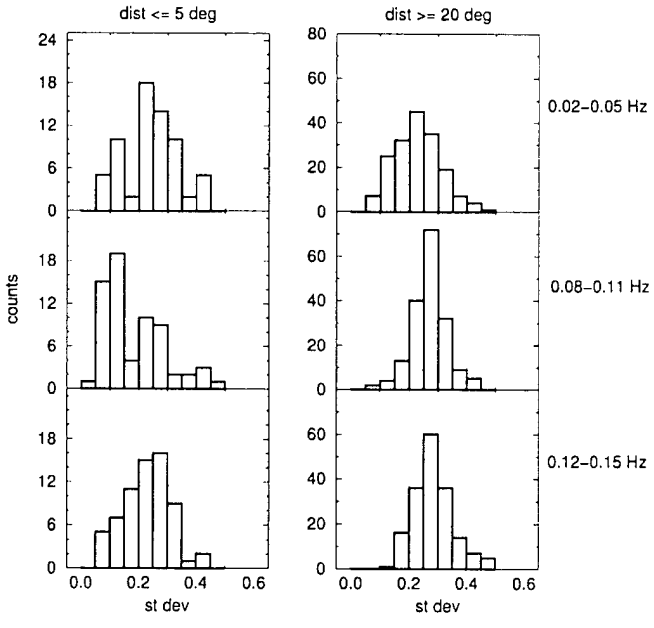

Figure 11. Histograms of standard deviations of the mean station $\log M_0$ estimated in three frequency bands (shown on right), for small and larger distances (shown on top).

The above estimates were compared in order to select the most suitable frequency bands, possibly varying with distance. Ideally, the corrected spectra would be flat over an extended band of frequencies. Flatness is particularly expected for explosions, as supported (within limits) by the explosion examples in Figure 9 above. The magnitude spectra estimated over any reasonable band would be then consistent. In reality, truly flat spectra over extended frequency bands are rare, so we need to choose bands small enough not to include too many variable features of the spectra, yet large enough not to reflect only local, possibly spurious, characteristics.

In view of the above, the two main desirable properties of a spectrum over a given frequency band are small standard deviations and flatness. For this reason, in our search for optimum frequency bands we used two criteria. First, small standard deviations from (1) above represent one measure of the suitability of a frequency band. Figure 11 indicates that for small distances, the 0.08-0.11 Hz frequency band may be preferable (the largest number of small standard deviations) to either 0.02-0.05 Hz, or 0.12-0.15 Hz. Larger distances do not present a clear picture, but it is still evident that relatively more small standard deviations are found in the 0.02-0.05 Hz frequency band, compared with the higher frequencies. We note that at this stage we do not use the standard deviations from (2), since they are designed to greatly diminish the presence of outliers and are thus not representative enough of the quality of the estimates in the different frequency bands. However, once a suitable frequency band is chosen, the robust mean is the most reliable estimate of $\log M_0$. Spectral flatness as measured with the slopes of the "robust" lines in (4) above provides a second measure of the quality of frequency band; the smaller the slope, the flatter the spectra. Table 1 shows examples of selected estimates, over one specific frequency band out of 153 (0.05-0.1 Hz), for the explosion and earthquake spectra shown in Figure 9. Smaller slopes (flatter spectra) are evident for explosions compared with earthquakes. On the other hand, increasing absolute values of slopes and standard deviations are seen for earthquakes with increasing distance. This is to be expected, as the relatively high-frequency band in the example is less suitable as distance increases.

Table 1. Station LogM0 estimates in 0.05-0.10 Hz from the spectra in Figure 9.

Event Type	*ID.station*	*Distance, degrees*	*Station $\log M_0$ (simple)*	*Station $\log M_0$ (robust)*	*Station slope/$\log M_0$*	m_b
Explosions	21450528.WMQ	2.2	14.31+0.10	14.33+0.08	+1.02/14.31	4.5
	21450535.MAK	7.1	15.60+0.15	15.67+0.05	+0.41/15.64	5.8
	21450534.ESDC	66.8	14.95+0.22	15.02+0.09	+1.62/14.97	5.4
Earthquakes	21456615.WMQ	0.4	13.92+0.14	14.01+0.05	+3.64/13.93	3.2
	21456712.ARU	22.2	14.44+0.25	14.44+0.24	-8.70/14.48	3.8
	21457058.ILAR	65.3	15.55+0.27	15.45+0.10	-11.18/15.59	4.3

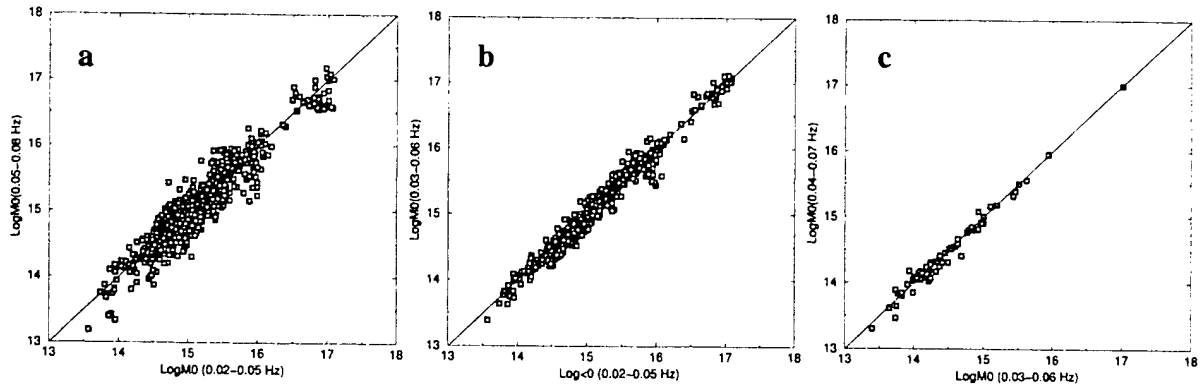

Figure 12. Comparison of station spectral magnitudes in different frequency bands: (a) adjacent bands, all distances; (b) overlapping bands, all distances; (c) overlapping bands, distances $\leq 5^{\circ}$.

Next, we examined the consistency of spectral magnitude estimates in different frequency bands. Figure 12 shows examples of such estimates in several frequency bands (marked along the plot axes). These results indicate that although measurements are generally consistent when measured in different frequency bands, some individual measurements do change significantly. Also, there is a tendency for measurements to be smaller at higher frequencies (points lie slightly to the right of the lines in Figure 12). These results indicate that spectral magnitudes can be measured in different frequency bands, but with some caution and attention to spectral shape variations.

Finally, we examine which frequency bands perform best for discrimination between small earthquakes and explosions. That is, we want to find out if any set of variable frequencies would perform better in terms of discrimination than a single frequency band applied at all distances. Figure 13 shows $\log M_0$:m_b plots using a set of variable frequencies (0.02-0.05 Hz for distances exceeding 25^0, 0.06-0.09 Hz for 10^0 to 250, and 0.08-0.11 Hz for distances below 10^0) and the 0.03-0.07 Hz frequency band for all distances. The plot on the left, where higher frequencies are used at small distances (and hence for the smallest earthquakes) apparently has a lower discriminating power for small events than when 0.03-0.07 Hz magnitudes are used. The reason is that the spectral magnitudes of smaller events ($\log M_0$ 14 to 15; i.e., M_s 2.2 to 3.2), recorded predominantly at regional distances, are generally smaller than the estimates at lower frequencies. We examined the $\log M_0$:m_b ratio for a number of frequency bands and established that the 0.03-0.07 Hz interval performs best in discriminating between earthquakes and explosions for the Lop Nor data set. The performance of the time domain M_s:m_b discriminant for these events (not shown), is similar to that of the variable frequency measurement (Figure 13, left), although the comparison is complicated by the fact that there is not a standard procedure for measuring time domain M_s in the regional distance range.

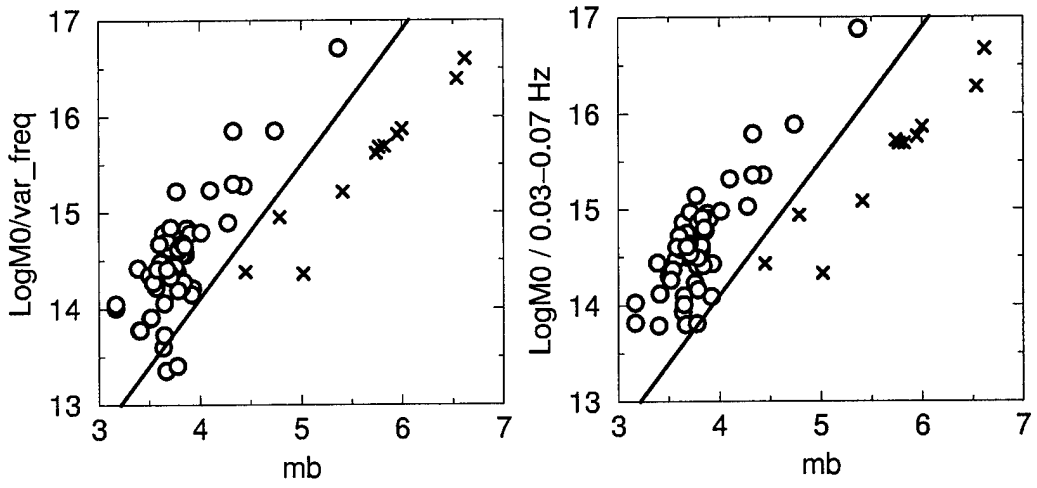

Figure 13. LogM_0:m_b plots showing event spectral magnitudes for earthquakes (O) and explosions (X) in Lop Nor. Station spectral magnitudes were calculated using frequencies increasing with distance (left) and the 0.03-0.07 Hz frequency band for all distances (right). Bold lines mark the empirical discrimination relationship of Stevens and McLaughlin (2001).

3.2 Path corrected noise estimates

While a path corrected spectral magnitude can be measured over any frequency band, it is subject to the following constraints:

1. Earthquake spectra decrease at high frequencies, depending on depth (Figure 6), so the high end of the frequency band should be low enough that discrimination is not degraded by this effect (Figure 13).

2. At high frequencies, attenuation is higher and the dispersion more variable, so the path correction is likely to be better and the signal may be higher at lower frequencies.

3. Noise increases at low frequency, so the low end of the frequency band should be at a frequency high enough to be above the noise level.

In order to quantify these effects better, we measured some "path corrected noise spectra" for the Lop Nor data set. These are simply noise spectra measured at the station that have been divided by an explosion Green's function in the same manner as would be done for a signal. Since the signal spectra are approximately flat over most of the frequency band, the path corrected noise spectra are a measure of the minimum path corrected signal that could be measured at each station.

Figure 14 shows the noise measurements for two stations: WMQ, located an average of 2 degrees from each event, and HIA, located an average of 27 degrees from each event. At the lowest frequencies, the noise levels decrease with increasing frequency, reaching a minimum at about 0.04 Hz, then increase to a peak at about 0.06 Hz, which corresponds to the frequency of the primary microseism peak. The noise levels then decline to about 0.1 Hz, and then increase. As Figure 14 shows, there is also substantial variability in the noise level, so that although the average noise level suggests that the minimum spectral magnitude that could be measured is about 13.5 at WMQ and 14.5 at HIA, it may be substantially lower or higher. These results suggest that in general it is best to measure surface wave spectra at frequencies above 0.03 Hz

and below 0.1 Hz. Although noise levels remain fairly low in the 0.1-0.2 Hz frequency band at the closest stations, factors #1 and #2 mentioned above make measurement in this band risky. Based on the empirical tests described earlier, we recommend measuring surface waves at frequencies between 0.03 and 0.08 Hz.

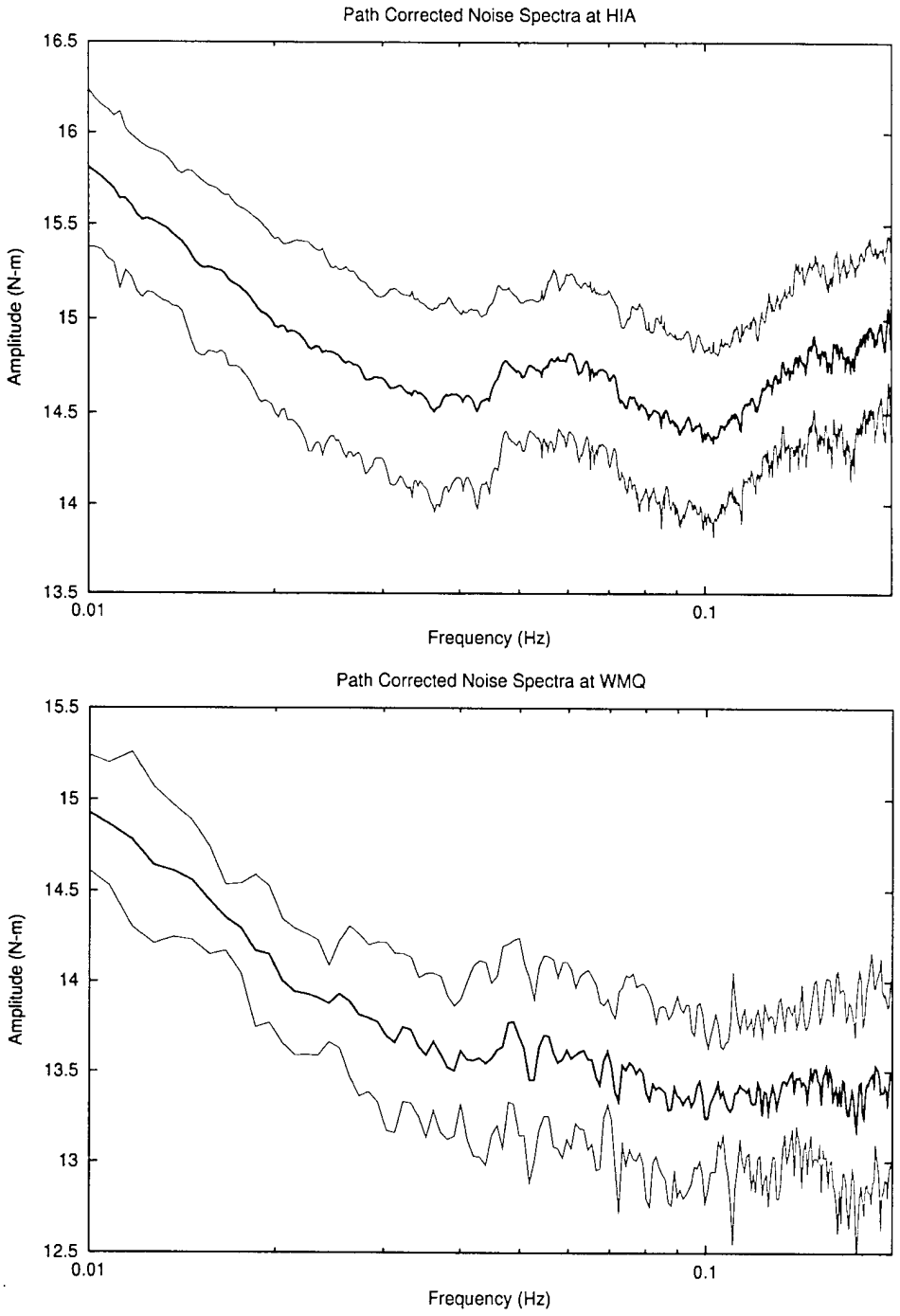

Figure 14. Average path corrected noise measurement and ±one standard deviation curves for 13 time segments at WMQ (bottom) and for 54 time segments at HIA (top). The average distance to WMQ is 2 degrees and the average distance to HIA is 27 degrees.

4. IMPROVED AZIMUTH ESTIMATION

To monitor nuclear testing, the International Data Center (IDC) automatically processes surface waves recorded at individual International Monitoring System (IMS) stations, attempting to identify them and measure amplitude and M_s. Three-component azimuth estimates derived using the current, spectral method are recorded but are too inaccurate to use for identification. That method is based on an algorithm originally proposed (Smart, 1978) as part of a surface wave detector, rather than as a means of estimating the azimuth. Selby (2000) suggested that another detection technique (Chael, 1997), based on correlation of the vertical and Hilbert transformed radial component Rayleigh wave records, could be used for azimuth estimation and would improve IDC processing.

To compare the performance of the algorithms, we incorporated the Chael/Selby (CS) algorithm into the automatic surface wave processing software that utilizes the current IDC method (CM). In the standard processing of surface waves, there is a detection if the surface waves pass a dispersion test (Stevens and McLaughlin, 2001). In this study, both algorithms are tested on 2,599 records that passed the dispersion test and 2,363 generally poorer S/N records that failed, all from events that had at least four surface wave detections. We assess the performance of each algorithm for different passbands and group velocity windows.

4.1 Differences between the algorithms

Both the CM and CS algorithms find the backazimuth that best matches the expectation that the horizontal and vertical components of the Rayleigh wave records are similar, but 90° out of phase. The biggest difference between algorithms is that the CM uses Love as well as Rayleigh waves to estimate the backazimuth.

The use of both Love and Rayleigh waves by the CM versus only Rayleigh waves by the CS algorithm makes it impossible to compare the algorithms using the same time window while optimizing the performance of both. The CS algorithm should perform optimally when the time window encompasses just the Rayleigh wave, as a longer window will only add noise. Antithetically, the CM should perform optimally with a longer time window that encompasses both the Rayleigh wave and the higher group velocity Love wave.

4.1.1 The Current Method

The CM finds values for r_n and l_n, the complex Fourier coefficients of the Rayleigh and Love wave vertical component displacements, ϕ, the backazimuth, and ε_n, the Rayleigh wave ellipticity, that minimize the squared distance between the data and model (Smart, 1978; 1981). The ellipticity may be assumed known, which reduces by one the degrees of freedom. Subscripts refer to frequency. The function minimized is written

$$\left|z_n - r_n\right|^2 + \left|y_n - \left(i\varepsilon_n r_n \cos(\phi) - l_n \sin(\phi)\right)\right|^2 + \left|x_n - \left(i\varepsilon_n r_n \beta + l_n \alpha\right)\right|^2 \qquad (1)$$

where x_n, y_n, and z_n are the complex Fourier coefficients of the east, north, and vertical components of the seismic record. Two important elements of this function are that the radial component of the Rayleigh wave equals $i\varepsilon_n r_n$, that is, the vertical component advanced by 90° and scaled by the ellipticity, and that the Love wave is independent of the Rayleigh wave.

4.1.2 The Chael/Selby algorithm and its implementation

The CS algorithm (Chael, 1997; Selby, 2000) finds the backazimuth for which the correlation coefficient of the vertical and Hilbert transformed radial is a maximum (Equation 2).

$$C_{z\bar{r}} = \frac{S_{z\bar{r}}}{\sqrt{S_{zz}S_{\bar{r}\bar{r}}}}, \tag{2}$$

where,

$$S_{jk} = \sum_{\tau=1}^{N} x_j(\tau)x_k(\tau). \tag{3}$$

The implementation uses the correlation of the Hilbert transformed vertical with the radial, for one degree increments of backazimuth. While Selby uses the maximum positive correlation as the backazimuth, Chael (1997) uses the central azimuth, determined by the circular mean (e.g. Fisher, 1993). We test the algorithm using both measures.

For synthetic Rayleigh waves with azimuthally evenly distributed random noise, the circular mean provides more accurate estimates than the maximum correlation. The lower the S/N, the greater the advantage of the circular mean.

For noise free data (i.e. synthetics), equation 2 will return a negative or positive constant, as the cross-correlation of the Hilbert transformed vertical and radial and the autocorrelation of the radials change in synch as the algorithm steps through backazimuths. Our implementation of the algorithm therefore provides two methods of estimating the similarity of the components. One uses the correlation coefficient (equation 2). The second method is intended to avoid the problem described above when data are noise free by normalizing by S_{zz} alone (equation 4).

$$C_{z\bar{r}} = \frac{S_{z\bar{r}}}{S_{zz}}. \tag{4}$$

4.2 Performance of the algorithms in 4 frequency bands.

The first set of tests used a 2.5 to 5.0 km/sec group velocity window, which should encompass both Love and Rayleigh waves, and compared backazimuth estimates in 3 relatively narrow, overlapping frequency bands, 0.02-0.04 Hz, 0.03-0.05, 0.04-0.06 Hz, plus one frequency band covering the entire spectrum from 0.02 to 0.06 Hz.

Figure 15 shows histograms of azimuth residuals for the CM and one implementation of the CS algorithm for the middle frequency band. Table 2 presents the errors associated with each method. The CS algorithm performs better in two ways. First, the CM applied as it is currently used in the automatic processing, has sign errors for a significant number of events. Second, the histograms reveal a much larger number of outliers for the CM compared to the CS algorithm.

Surprisingly, the best implementation of the CS algorithm is the combination of the peak position of the correlation and normalization of the correlation by $\sqrt{S_{zz}S_{\bar{r}\bar{r}}}$. Why the maximum

correlation provides a more accurate estimate of backazimuth than the circular mean bears further investigation. One possibility is that the real noise is azimuthally unevenly distributed and so biases the circular mean measurement toward the direction of the predominant noise source. Such skewed noise would not so strongly affect the maximum correlation position.

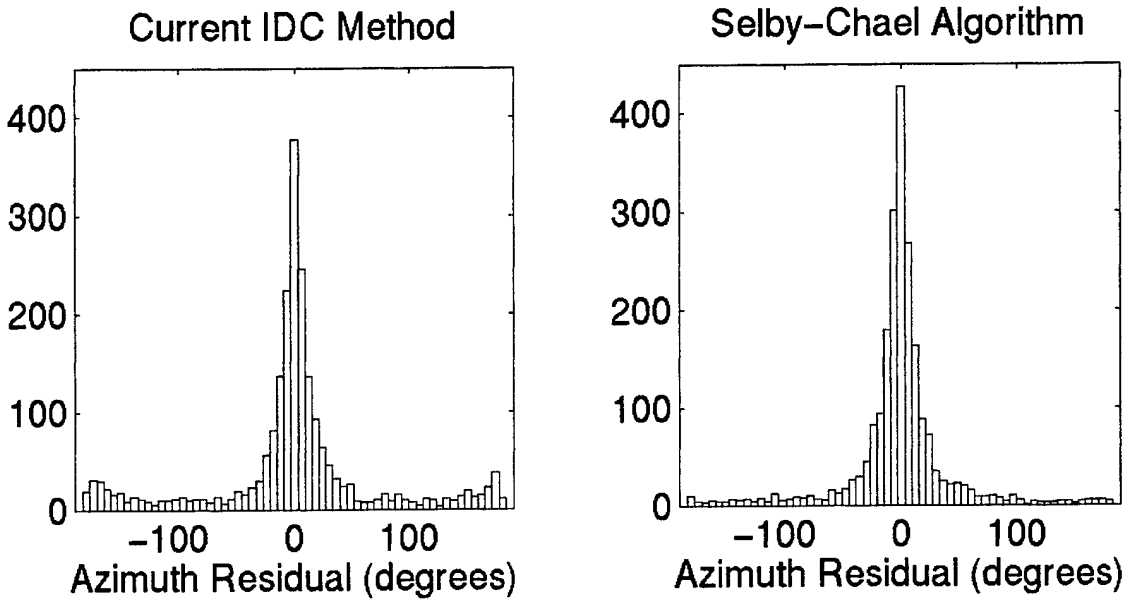

Figure 15. Azimuth residuals for 0.03-0.05 Hz using the current method (left) and the Chael/ Selby algorithm using the normalization of equation 2 and peak correlation (right).

The scaled median absolute deviation (SMAD), the one-norm measure of the central tendency, provides a more accurate measure of the spread of data about the central value for such heavy-tailed data as these than does the standard deviation (STD). Errors for all of the tests performed badly fail the Kolmogorov-Smirnov test for normality of a distribution. That the STDs are so much larger than the SMADs indicates that, while most estimates are reasonably accurate, there are a large number of outliers.

The CM performs best at higher frequency, while the CS algorithm performs best at lower frequency. The CM performs almost as well as the CS algorithm at the highest frequencies tested. This is likely because the Love waves are relatively larger at longer periods than the Rayleigh waves, and contrary to expectations, the CM performs poorly when the Love waves are very large. This is probably due to the 180 degree ambiguity in Love wave polarization, which causes large Love wave amplitudes to increase the likelihood of a 180 degree error in azimuth.

Larger azimuth residuals at higher frequency for the CS method may be due to lower S/N. Alternately, greater lateral heterogeneity in the shallower Earth layers could lead to more variation in the propagation direction of higher frequency surface waves. The estimates may in that case accurately reflect the effect of lateral heterogeneities on higher frequency waves.

For the CS algorithm, the backazimuth residuals for the broader frequency band are comparable to those in the 0.03-0.05 Hz passband, larger than those of the lowest frequency passband, and smaller than those of the highest frequency passband. The parts of the frequency band where the backazimuth either varies or is less well resolved appear to diminish resolution of the broadband

estimate compared to narrower passband estimates, so a broad frequency band does not provide any advantage. For the CM, the performance is actually poorer for the broadband data than for each of the narrower passbands used. The rest of the analyses are performed for just the three narrow frequency bands.

Table 2. Scaled median absolute deviations and standard deviations (in parentheses) of the azimuth residuals in 4 frequency bands from the algorithms tested. Four variations of the implementation of the CS algorithm are tested. CS_1 and CS_2 use the peak amplitude of the correlation while CS_3 and CS_4 use the circular mean. CS_1 and CS_3 are normalized by $\sqrt{S_{zz}S_{\overline{rr}}}$ as in equation 2. CS_2 and CS_4 are normalized by S_{zz} as in equation 4.

	.02-.04 Hz	.03-.05 Hz	.04-.06 Hz	.02-.06 Hz
CM	31 (85)	22 (71)	22 (64)	20 (68)
CS1	13 (41)	16 (47)	19 (53)	16 (45)
CS2	17 (40)	19 (46)	22 (52)	20 (45)
CS3	15 (39)	17 (46)	20 (52)	17 (45)
CS4	17 (40)	19 (46)	22 (53)	20 (45)

4.3 The effect of signal strength (event size) on backazimuth estimates.

Figure 16 shows the backazimuth residuals for each of the algorithms vs. event size, which serves as a proxy for the signal-to-noise ratio. The CM is almost comparable in performance to the CS algorithm for large events, except for a large number of outliers at 180 degrees. It begins to fail badly for smaller events, especially at the lowest frequencies. Table 3 show results comparable to Table 2, but for events of M_s 5.0 and above.

Table 3. Same as Table 2, but for 335 records of events with $M_s \geq 5.0$.

	.02-.04 Hz	.03-.05 Hz	.04-.06 Hz
CM	14.5 (68.6)	14.4 (51.9)	12.9 (47.3)
SC_1	8.7 (30.5)	9.6 (29.8)	10.6 (35.2)
SC_2	10.8 (29.5)	13.0 (28.4)	13.4 (34.5)
SC_3	9.4 (29.7)	11.7 (28.9)	12.2 (34.9)
SC_4	10.7 (29.5)	12.8 (28.4)	13.2 (34.5)

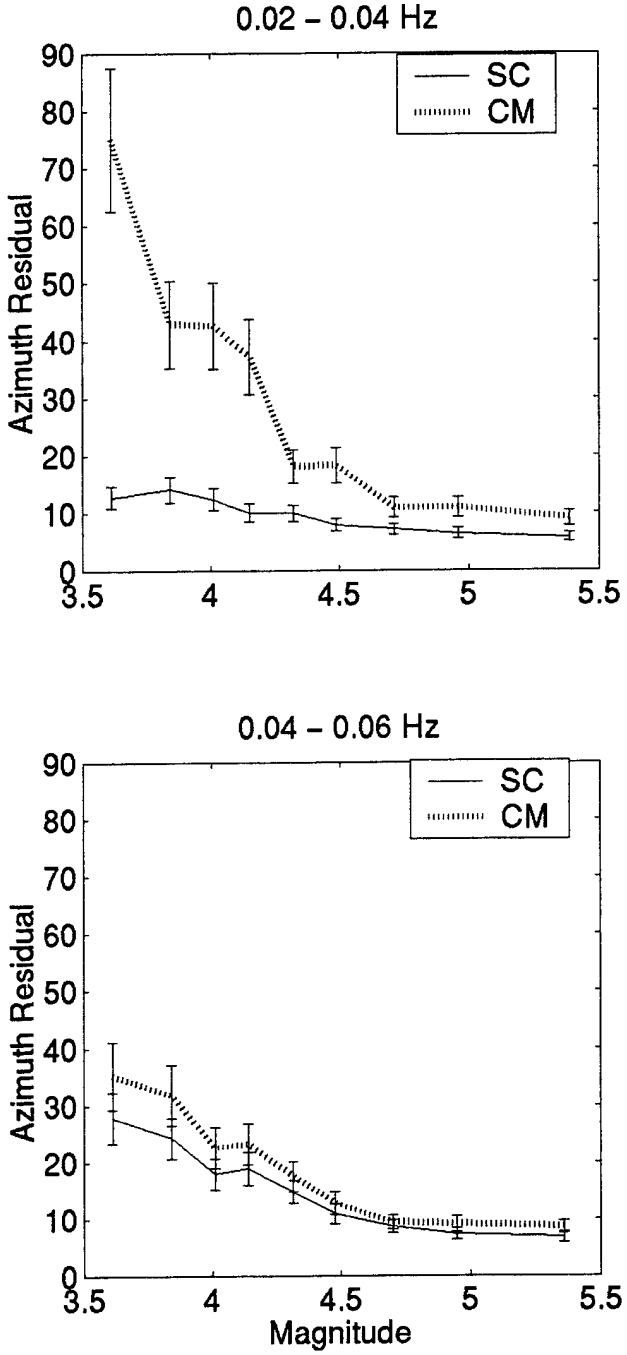

Figure 16. Median ±2 SMAD confidence intervals of azimuth residuals binned by M_s values, for the CM (dotted) and the best performing implementation of the CS algorithm (solid). Each bin has approximately 250 azimuth residuals. Results in the 20-33 second period passband are intermediate between those shown.

4.4 Variable group velocity

The work reported above used 2.5 to 5.0 km/sec group velocity windows that we expect to favor the CM, as they are most likely to include both Love and Rayleigh waves. Next we use the group velocities predicted by a 1° global surface wave model (Stevens, et al 2002) to select windows intended to more narrowly bracket the Rayleigh waves and so minimize the effect of noise outside those windows (Figure 17). The minimum group velocity is that used in the dispersion test for surface waves at the high frequency corner of the passband. Similarly, the maximum group velocity is determined by the low frequency corner.

Table 4 is similar to Table 2, but for the variable length group velocity windows. The performance of the CM is slightly worse for the shorter windows at the highest frequency passband, as expected, and there is a small improvement in performance for the best performing algorithm, CS using the peak of the correlation with normalization by $\sqrt{S_{zz}S_{rr}}$, compared to the longer group velocity windows. Overall, the effect of narrowly isolating the Rayleigh waves is quite small, which is encouraging regarding the prospects of the CS algorithm for routine detection.

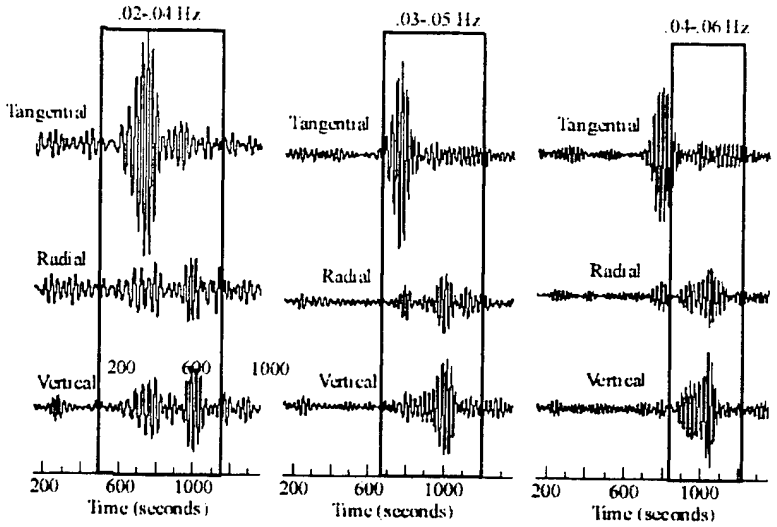

Figure 17. Surface wave records in the 3 passbands tested at the station ARCES for an Ms 5.0 event at 6035 km. The entire trace is the 5.0 to 2.5 km/s group velocity window, while the outlined segments are the shorter group velocity windows used to isolate the Rayleigh waves. The isolation works best at the highest frequency passband, where the large Love wave (top trace) is outside the narrower window.

Table 4. Same as Table 2, but for group velocity windows designed to isolate the Rayleigh waves. The change from the 2.5 to 5 km/s group velocity windows is given in parentheses (negative change is improvement).

	.02-.04 Hz	.03-.05 Hz	.04-.06 Hz
CM	31.4 (+0.7)	21.2 (-0.4)	23.9 (+1.5)
SC_1	12.7 (-0.5)	14.9 (-0.8)	18.1 (-0.5)
SC_2	17.0 (+0.5)	19.0 (+0.3)	21.5 (-0.3)
SC_3	14.7 (-0.1)	16.8 (-0.2)	19.6 (-0.4)
SC_4	16.9 (+0.4)	19.0 (+0.2)	21.6 (-0.2)

4.5 Predicting accuracy of estimates using the crosscorrelation value

The crosscorrelation of the Hilbert transformed vertical with the radial predicts the accuracy of the azimuth estimate. Figure 18 shows azimuth estimate residuals vs. the cross-correlation for the best implementation of the CS algorithm applied to data that pass the dispersion test.

For 0.02 to 0.04 Hz, 60% of the data have a cross-correlation ≥ 0.8. The SMAD of the error of those data is 8.5°, vs. 12.7° for all the data. For 0.03 to 0.05 Hz, 58% of the data have a crosscorrelation value ≥ 0.8, and those data have a smad of 9.3° vs 14.9° for all the data. For 0.04 to 0.06 Hz, 54% of the data have a crosscorrelation value ≥ 0.8, and those data have a smad of 11.1° vs 18.1° for all the data.

This ability to predict backazimuth estimate accuracy can aid association with known events. In particular, the strict dispersion criteria for detection at the IDC could be relaxed in cases where the backazimuth is consistent with the theoretical backazimuth and the crosscorrelation value is high. Well constrained uncertainties are also important for understanding the accuracy of inferences made from measurements of the surface waves, for example, tomography based on surface wave polarization (e.g. Yoshizawa, et al., 1999).

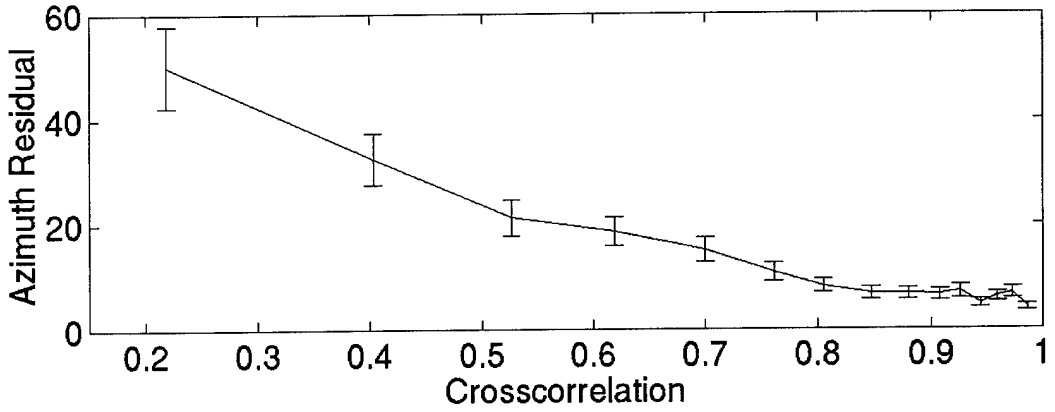

Figure 18. Median azimuth residuals ±2 SMAD confidence intervals vs. the median cross-correlation of the radial and Hilbert transformed vertical Rayleigh waves, for each bin of 171 measurements, for the 0.03-0.05 Hz passband. Results are similar for the other passbands.

4.6 Events for which surface waves are not detected

Figure 19 shows the results of each method of polarization analysis applied to the poorer S/N records that did not pass the dispersion test. The CS method (implemented using maximum cross-correlation) extracts accurate backazimuth estimates for many of these data. The more accurate estimates can be identified by their cross-correlation value.

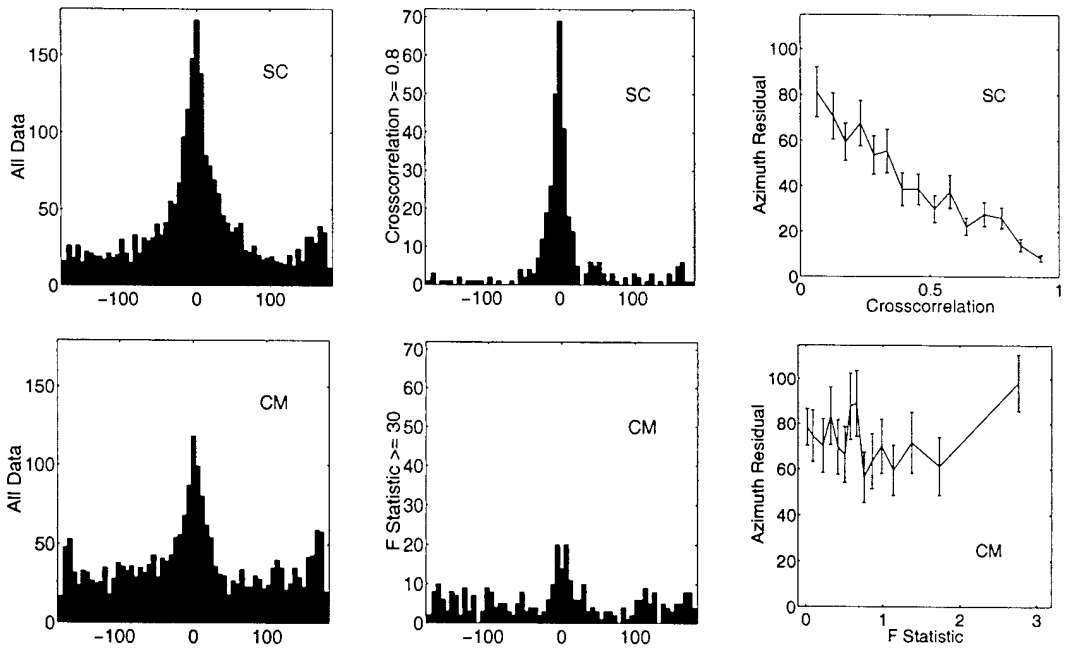

Figure 19. Azimuth residuals for the 0.02 – 0.04 Hz passband for the CS algorithm (top row) and the CM (bottom row). Histograms of azimuth residuals for all the data (left column) and for data with correlation ≥ 0.8 for CS (upper middle) or F-statistic ≥ 30 for the CM (lower middle). The central plots use ~14.5% of the data in each case. The upper right plot shows the median azimuth residual ±2 SMAD confidence intervals vs. the correlation, as in Figure 18, for the CS algorithm. The bottom right shows the median azimuth residual ±2 SMAD confidence vs. the F statistic of the CM.

The SMAD of the azimuth residuals for data not passing the dispersion test is 58°, vs. 108° for the CM. The upper central plot shows histograms just for data with a correlation ≥ 0.8, which comprise 14.7% of the data. Their azimuth residual has a SMAD of 14.8°. The F-statistic of the CM does not provide similar predictive capabilities. In fact, for the largest F-statistic values, the CM's error increases. This is because the F-statistic can be very large when the signal is dominated by very large Love waves, but such records often have 180° (i.e. sign) errors. Even disregarding the sign errors, the F-statistic is a much poorer predictor of the accuracy of polarization estimates, and the resolution of the current method is much poorer than that of the CS algorithm.

4.7 Conclusions of Azimuth Study

The correlation of the radial and Hilbert transformed vertical seismic records provides accurate estimates of Rayleigh wave polarization and provides significant improvement over the current method employed at the IDC. Further, the value of the cross-correlation provides a reliable estimate of the accuracy of the polarization.

The CS method could also improve detection of Rayleigh waves, through better association with known events. Specifically, current strict IDC requirements on detection in multiple passbands could be relaxed when there is a backazimuth estimate that has a high cross-correlation value and is consistent with the theoretical backazimuth.

5. CONCLUSIONS AND RECOMMENDATIONS

Improvements to surface wave dispersion models are being accomplished by: 1) continuing addition of new data with good quality control and particular attention to regions with gaps in data coverage; 2) removal of poor quality data in the data set (poor quality data becomes more apparent as the data set increases and the model quality improves); 3) addition of model types where the data requires them; 4) improvement in constraints on sediments and Moho thickness; 5) improvement to the regularization techniques, which can now be defined on a model by model basis, allowing improved data fit while achieving realistic earth models.

Improved methods for surface wave measurement are being implemented and tested. Surface wave spectra are derived from phase-matched filtered data, and the phase-matched filters are derived from the regionalized dispersion models. Path corrected spectral magnitudes are derived by dividing the observed spectra by an explosion Green's function, where the Green's functions are calculated from the global earth models. Thus we use the earth and dispersion models to optimize spectral measurements and regionalize surface wave excitation and attenuation. In this paper, we have described a detailed study of procedures for optimizing measurement of path corrected spectral magnitudes. A significant advantage of $\log M_0$ over M_s is that it can be measured at any distance range without the anomalies caused by variations in dispersion that affect M_s. In principle, $\log M_0$ can be measured over any frequency band and optimized by choosing the band with maximum S/N. However, we found that $\log M_0$ for earthquakes is frequently significantly lower at higher frequencies, which degrades discrimination, and that furthermore the S/N for lower frequencies is good even for very short distances. We therefore recommend that surface wave measurements be made at lower frequencies even at short distances. We are in the process of determining the optimum frequency band for measurement, and our current recommendation is to use a frequency band of 0.03-0.07 Hz consistently for all data. We are continuing to evaluate this recommendation for a larger data set with more types of earth structure.

6. DATA DELIVERABLE

Two data deliverables are provided together with this annual report. They are:

1. The current set of earth models, dispersion curves and other derived data. These are contained in compressed tar file "LP_2003_Oct.tar.Z". Information on data format is included in the delivery.

2. The maxpmf program compiled for Sun Solaris, and the maxpmf man page. These are contained in compressed tar file "maxpmf_5.2.tar.Z"

These data deliverables may be obtained from the contracting office or from the authors.

REFERENCES

Bassin, C., G. Laske, and G. Masters (2000), The Current Limits of Resolution for Surface Wave Tomography in North America, *EOS Trans AGU* 81, F897.

Chael, E. (1997), An automated Rayleigh-Wave Detection Algorithm, B.S.S.A., **87**, 157-163.

Ekstrom, G., A. M. Dziewonski, G. P. Smith, and W. Su (1996), Elastic and Inelastic Structure Beneath Eurasia, in *Proceedings of the 18th Annual Seismic Research Symposium on Monitoring a Comprehensive Test Ban Treaty, 4-6 September, 1996*, Phillips Laboratory Report PL-TR-96-2153, July, ADA313692, 309-318.

Engdahl, E. R., R. van der Hilst, and R. Buland (1998), Global Teleseismic Earthquake Relocation with Improved Travel Time and Procedures for Depth Determination, *Bull. Seismol. Soc. Am.* 88, 722 - 743.

Fisher, N.I. (1993), Statistical Analysis of Circular Data, Cambridge Univ. Press.

Hansen, P. C. (1998), Rank-Deficient and Discrete Ill-Posed Problems, SIAM, Philadelphia, 1998.

Huang, Z., W. Su, Y. Peng, Y. Zheng, and H. Li (2003), Rayleigh Wave Tomography of China and Adjacent Regions. *J. Geophys. Res.* 108(B3), 2073, doi: 10.1029/2001JB001696.

Kennett, B. L. N. E. R. Engdahl, and R. Buland (1995), Constraints on Seismic Velocities in the Earth from Travel Times, *Geophys. J. Int.* 122, 108-124.

Laske, G. and G. Masters (1997), A Global Digital Map of Sediment Thickness, *EOS Trans. AGU* 78, F483.

Laske, G., G. Masters, and C. Reif, Crust 2.0 (2001): A New Global Crustal Model at 2x2 Degrees, http://mahi.ucsd.edu/Gabi/rem.html.

Levshin, A., J. L. Stevens, M. H. Ritzwoller, and D. A. Adams (2002), Short Period (7s-15s) Group Velocity Measurements and Maps in Central Asia, in *Proceedings of the 24th Annual DOD/DOE Seismic Research Symposium, 17-19 September 2002*, 97-106.

Levshin, A. L., J. L. Stevens, M. H. Ritzwoller, D. A. Adams, and G. E. Baker (2003), "Improvement of Detection and Discrimination Using Short Period (7s-15s) Surface Waves in W. China, N. India, Pakistan and Environs," Final report submitted to Defense Threat Reduction Agency, SAIC Report No. 03/2008, CU Project No. 1532378, April.

Marshall, P. D. and P. W. Basham (1972), Discrimination Between Earthquakes and Underground Nuclear Explosions Employing an Improved M_s Scale, *Geophys. J. R. astr. Soc.* 28, 431-458.

Mooney, W., G. Laske, and G. Masters (1998), Crust 5.1: A Global Crustal Model at 5x5 Degrees, *J. Geophys. Res.* 103, 727-747.

Selby, N.D. (2000), Identification, Association, and Analysis of Rayleigh Waves in a CTBT Monitoring Context, Proceedings of the 22nd Annual DOD/DOE Seismic Research Symposium, 12-15 September, 2000.

Smart, E. (1978), A three-component, single-station, maximum-likelihood surface wave processor, *Geotech Report No.* SDAC-TR-77-14.

Smart, E. (1981), Regional phase processors, *Geotech Report No.* VSC-TR-81-19.

Stevens, J. L. and D.A. Adams (2000), Improved Surface Wave Detection and Measurement Using Phase-Matched Filtering and Improved Regionalized Models, in *Proceedings of the 22nd Annual DOD/DOE Seismic Research Symposium, 12-15 September 2000*, 145-154.

Stevens, J. L., D.A. Adams, and G. E. Baker (2001a), Improved Surface Wave Detection and Measurement Using Phase-Matched Filtering with a Global One Degree Dispersion Model, in *Proceedings of the 23rd Annual DOD/DOE Seismic Research Symposium, 1-5 October 2001*, 420-430.

Stevens, J. L., D. A. Adams, and E. Baker (2001b), *Surface Wave Detection and Measurement Using a One Degree Global Dispersion Grid*, SAIC Final Report to Defense Threat Reduction Agency, SAIC-01/1084, December.

Stevens, J. L., D. A. Adams, and E. Baker (2002), Improved Surface Wave Dispersion Models and Azimuth Estimation Techniques, in *Proceedings of the 24th Annual DOD/DOE Seismic Research Symposium, 17-19 September 2002*, 552-561.

Stevens, J. L. and K. L. McLaughlin (2001), Optimization of Surface Wave Identification and Measurement, *Pure Appl. Geophs.* 158, 1547-1582.

Yang, X., S. R. Taylor, H. J. Patton, M. Maceira, and A. A. Velasco (2002), Evaluation of Intermediate-Period (10- to 30-sec) Rayleigh-Wave Group Velocity Maps for Central Asia, in *Proceedings of the 24th Annual DOD/DOE Seismic Research Symposium, 17-19 September 2002,* 609-617.

Yoshizawa, K., K. Yomogida, and S. Tsuboi, 1999, Resolving power of surface wave polarization data for higher-order heterogeneities, Geophys. J. Int., **138**, 205-220.